PHYSICAL REVIEW B VOLUME 52, NUMBER 3 15 JULY 1995-I

Ballistic-electron-emission-microscopy investigation of hot-carrier transport in epitaxial $CoSi_2$ films on Si(100) and Si(111)

E. Y. Lee, H. Sirringhaus, U. Kafader, and H. von Känel
Laboratorium für Festkörperphysik, Eidgenössische Technische Hochschule Zürich, CH-8093 Zürich, Switzerland
(Received 19 December 1994; revised manuscript received 1 March 1995)

The attenuation lengths λ's of hot electrons in thin films of epitaxial $CoSi_2$ on Si(100) and Si(111) were measured as a function of energy using constant-height-mode and constant-current-mode ballistic-electron-emission microscopy (BEEM). Between ~1 and ~3 eV above the Fermi energy, the λ's were found to be significantly anisotropic and their energy dependencies differed strongly from the free-electron behavior. At higher energies, e^--e^- scattering in $CoSi_2$ was found to be dominant, giving a majority of the BEEM current and largely determining the spatial resolution of both forward and reverse BEEM imaging, both of which could be used for direct mapping of interfacial steps. Also, constant-height-mode BEEM was used to investigate the interfacial transport across $CoSi_2$/*n*-type Si(111), $CoSi_2$/*p*-type Si(111), and $CoSi_2$/*n*-type Si(100). Evidence for different interfacial structures of $CoSi_2$/Si(100) was observed.

I. INTRODUCTION

It has been more than six years since ballistic-electron-emission microscopy (BEEM) was first used to measure Schottky barrier height and to study the uniformity of the metal-semiconductor (*m-s*) interface,[1] and subsequent work established BEEM as a method for the characterization of the *m-s* interface as well as for the study of hot-carrier transport through the metal overlayer.[2] In a typical BEEM experiment, a scanning-tunneling microscope (STM) tip is used as an injector of electrons or holes into a metal overlayer on a substrate. When the tip is biased with respect to the overlayer, tunneling of electrons gives rise to a hot-carrier distribution in the overlayer, and the overlayer is made thin enough so that a significant fraction of the injected charge carriers travel across it to be incident upon the *m-s* interface. A fraction of the incident carriers are transmitted into the substrate if (1) there are final states available in the substrate, and (2) the kinematic constraints governing the particular *m-s* interface are satisfied. The current collected in the substrate is called the BEEM or the ballistic-electron-emission-spectroscopy (BEES) current, depending on whether the emphasis is on microscopy or spectroscopy. One can draw an analogy to a transistor, and think of the STM tip as an emitter, the metal overlayer as a base, and the substrate as a collector. We will use this convention, and refer to the metal overlayer as the base and the BEEM current as the collector current I_c.

In addition to studying the Schottky-barrier height and the interfacial uniformity, BEEM can also be used to study the energy-dependent hot-carrier scattering in the base and the energy-dependent transmission probability across the *m-s* interface. The attenuation lengths λ's of hot electrons for PtSi/Si(100),[3] Au/Si(100),[4] Pd/Si(111),[5] Au/GaP(110),[6] and Mg/GaP(110) (Ref. 6) have already been measured by BEEM. The measured λ's were used to infer the inelastic mean free path lengths λ_i's, using transport modeling such as Monte Carlo simulation.[6,7] Free-electron-like band structures were assumed for the metals studied, and adequate phenomenological descriptions of the data could be found by variation of the parameters associated with a free-electron theory[8] of e^--e^- scattering.

Previously, we reported performing *in situ* BEEM at 77 K on epitaxial $CoSi_2$/*n*-type Si(111) grown by molecular-beam epitaxy (MBE).[9,10] We also measured the λ of hot electrons along the ⟨111⟩ direction in $CoSi_2$ using a constant-height (CH) mode[11] BEEM.[10] We have now also done measurements of λ along the ⟨100⟩ direction on epitaxial $CoSi_2$/*n*-type Si(100), and the two λ's are found to be quite different. In this paper, we will make a quantitative comparison between the two λ's, and also compare the λ's to a free-electron theory of e^--e^- scattering. It will be shown that the observed behavior is clearly non-free-electron-like.

For $CoSi_2$/*n*-Si(111), in the higher-energy range, secondary electrons created in the base were found to be significant, even forming the majority fraction of the BEEM current and changing the transport through the base from ballistic to diffusive.[12] By performing reverse BEEM spectroscopy[13] on $CoSi_2$/*p*-type Si(111), the contribution of secondary electrons generated either in the base or in the Si could be estimated, and reverse BEEM imaging showed that most of the secondaries were generated in the base rather than in the Si.

We also performed CH-mode BEEM for $CoSi_2$/*n*-type Si(111), $CoSi_2$/*p*-type Si(111), and $CoSi_2$/*n*-type Si(100) to study the transport across these *m-s* interfaces. In CH-mode BEEM, the effect of the unknown tunnel-current distribution is eliminated as much as possible.[11] We will discuss the observations in terms of $k_\parallel$ and energy conservation.[1] During our study, at least two different kinds of interfacial structures of $CoSi_2$/*n*-type Si(100) were detected by BEEM, consistent with a previous TEM investigation of this interface.

An outline of this paper is as follows. First, an intro-

 ©1995 The American Physical Society

duction to transport processes in BEEM will be given in Sec. II A, and this will be followed by a brief description of CH-mode BEEM. Next, a result from a free-electron theory of e^--e^- scattering will be presented and applied to $CoSi_2$, Au, and Al in Sec. II C, and the attenuation length will be discussed. In Sec. III, the experimental procedure will be described. In Sec. IV A, comparisons will be made between the spectra for $CoSi_2$/*n*-type Si(111) and $CoSi_2$/*p*-type Si(111). Next, comparisons between the spectra for $CoSi_2$/*n*-type Si(111) and $CoSi_2$/*n*-type Si(100) will be made. The electron attenuation lengths for the ⟨100⟩ and ⟨111⟩ directions of $CoSi_2$ will be discussed next, and the paper will conclude after a consideration of the spatial distribution of charge carriers and the role of the secondary charge carriers in BEEM.

II. THEORY AND BACKGROUND

A. Introduction to transport processes in BEEM

In discussing BEEM, it will be convenient to separate various transport processes and to define certain terms. There were many BEEM theories[1,11,14–16] that were developed within the last decade, and, rather than describing each in detail, it would be more useful to talk in general terms in anticipation of the much more specific discussion later in this paper dealing with the transport physics of epitaxial $CoSi_2$/Si. For a more detailed overview of transport processes in BEEM, the reader is referred to Ref. 2.

The initial process in BEEM is the injection of electrons or holes by the STM tip into the metal base. The distribution of the tunnel current, $P(E,k_\parallel)$, in the base is very important and will be brought up numerous times. Integrating P, one obtains the tunnel current, I_t, which is held constant in the conventional BEEM. In Sec. II B, another mode of BEEM will be discussed that eliminates as much as possible the dependence of BEEM on the unknown $P(E,k_\parallel)$.

Within the base, injected hot carriers travel until they (1) undergo elastic scattering from impurities or defects, (2) undergo semielastic scattering from phonons, (3) undergo e^--e^- scattering (one can just as well talk about *h*-*h* scattering), or (4) cross the *m*-*s* interface. The scattering from defects can be observed by BEEM and it is one of the technological motivations for this technique. In principle, defects can be minimized. Phonon scattering in a metal appears to be insignificant in comparison to e^--e^- scattering for hot carriers, just a few tenths of an eV away from the Fermi energy E_F. When e^--e^- scattering occurs, an injected carrier loses some of its energy and momentum and excites electron-hole pair(s) from the metal Fermi sea. It is convenient to talk in terms of the primary current injected by the STM tip and the secondary current generated in the base. In a free-electron-like system, it can be shown that a typical electron loses $\frac{2}{3}$ of its excitation energy above E_F after an e^--e^- scattering.[8] The secondary current[13] can contribute to the collector current (BEEM current) I_c, and it will be demonstrated below that it is quite important at high energies.

Other considerations for the base are quantum effects, be it quantum-size effects (QSE's) or transport through superlattices. Formation of quantized subbands due to QSE's in epitaxial thin films of $CoSi_2$ were observed by current-imaging tunneling spectroscopy[17] and modulation spectroscopy,[12] and they were also found to influence the conventional BEEM spectrum slightly.[9] In this paper, QSE's in BEEM will not be discussed. Even though QSE's resulted in significant alteration of the local density of states (LDOS) and hence of $P(E,k_\parallel)$, it was found that QSE's could be neglected in analyzing the constant-height-mode BEEM data to be discussed in Sec. II B, because most of the change in dI_c/dV due to QSE's disappeared when this quantity was normalized by dI_t/dV. This topic will be dealt with elsewhere.

Another important process in BEEM is the transmission across the *m*-*s* interface. This probability is determined by the availability of the final states, e.g., Schottky-barrier and satellite bands, as well as by kinematic constraints due to energy and $k_\parallel$ conservation, which may hold to varying degrees. With full conservation and disregarding all complications, one essentially has the Bell-Kaiser (BK) theory,[1] which well fits the BEEM spectra for many *m*-*s* systems. A modified version adding in a dynamic effect of quantum-mechanical reflection has also been successfully used.[14] Non-$k_\parallel$-conserving theories also do well.[15,16]

For the collector, there are several ways to take into account the effect of the image force on the Schottky barrier. Some of BEEM theories[1,11,14,15] ignored the presence of band bending due to image force, whereas others[7] added a truncated-image potential to the potential of the Schottky barrier, thereby distinguishing the metallurgical interface and the actual Schottky-barrier height maximum, which may lie tens of Å away from the metallurgical interface.[18] Depending on the choice of the image potential or on the complete lack of it, one could obtain quite different transmission probabilities across the interface. Phonon scattering[7] and impact ionization in the substrate[6] are in principle relevant, but, for the interpretation of the results to be presented in this paper, they were found nonessential.

B. Constant-height-mode BEEM

The conventional BEEM can be called constant-current-mode (CC-mode) BEEM, because the tunnel current I_t is always maintained to be constant.[1] As described in Sec. II A, the collector current I_c is approximately proportional to I_t and is an integral over energy, so the unknown tunneling current distribution $P(E,k_\parallel)$ is very important. Although there now exist many theories dealing with STM tips, it would be desirable to perform BEEM in a way less sensitive to the tip condition. Just as importantly, the surface LDOS of the sample can have strong features that also affect $P(E,k_\parallel)$ directly. In addition, excitations and resonances in the tunnel junction can affect the tunneling process and alter $P(E,k_\parallel)$.[10]

Stiles and Hamann[11] proposed constant-height-mode (CH-mode) BEEM, in which the tip-sample separation is held constant during the taking of a BEEM spectrum and

the tunnel current I_t and the BEEM current I_c are measured simultaneously as a function of the tip-sample bias V. [In Eqs. (1)–(11), d is a constant.] This is exactly the same as scanning-tunneling spectroscopy,[19] but an additional quantity, namely I_c, is measured. As such, one has both the surface electronic structure and the BEEM component in the data.

In the Stiles-Hamann (SH) theory,[11] I_c takes the following form:

$$I_c = e\int_0^{eV} dE \prod t(E,k_\parallel,V,d)T(n,E,k_\parallel) \ , \quad (1)$$

where T is the transmission probability across the base into the substrate, and $t(E,k_\parallel,V,d)$ is the tunneling probability under the WKB approximation for an electron of energy E and $k_\parallel$ to tunnel across a planar-tunnel junction of thickness d, biased by a voltage V. The energy E is measured from the base Fermi energy E_F. $\prod$ is an integral operator defined as below, where the integration is over the interface Brillouin zone (IBZ), and n refers to all states with a given E and $k_\parallel$ in the base:

$$\prod = \int_{\mathrm{IBZ}} \frac{d^2k_\parallel}{(2\pi)^2} \sum_n \ . \quad (2)$$

The tunnel current I_t is

$$I_t = e\int_0^{eV} dE \prod t(E,k_\parallel,V,d) \ . \quad (3)$$

Because t, to a good approximation, is a function of $\omega = E + eV/2, (dt/dE) \approx (dt/d\omega)$ and $(dt/dV) \approx (e/2)(dt/d\omega)$, so that

$$\frac{dt}{dV} \approx \frac{e}{2}\frac{dt}{dE} \ . \quad (4)$$

Differentiating Eq. (3) with respect to V, using Eq. (4), and integrating by parts, one obtains

$$\frac{dI_t}{dV} \approx \frac{3e^2}{2}\prod t(eV,k_\parallel,V,d) - \frac{e^2}{2}\prod t(0,k_\parallel,V,d) \ . \quad (5)$$

Differentiating Eq. (1),

$$\frac{dI_c}{dV} = e\int_0^{eV} dE \prod \frac{dt(E,k_\parallel,V,d)}{dV} T(n,E,k_\parallel) + e^2 \prod t(eV,k_\parallel,V,d)T(n,eV,k_\parallel) \ . \quad (6)$$

In the SH theory which treats $V<0$, the second term in Eq. (5) and the first term in Eq. (6) are dropped, so that

$$\frac{dI_c/dV}{dI_t/dV} \approx \tfrac{2}{3}P \ , \quad (7)$$

where P is the transmission probability (TP) across the base into the substrate averaged over the IBZ. In Ref. 11, scattering in the base was neglected so that the TP was the same as the interfacial transmission probability (ITP) defined below as P_I in Eq. (8). In the zero-thickness limit, P is the same as P_I,

$$P_I \approx \prod W(eV,k_\parallel,V,d)T(n,eV,k_\parallel)) \ , \quad (8)$$

$$W(E,k_\parallel,V,d) = t(E,k_\parallel,V,d) \Big/ \prod t(E,k_\parallel,V,d), \quad (9)$$

where W is a normalized tunnel-current distribution that depends on the tip-sample separation, d, but only weakly on V at low voltages. (Under certain tunneling conditions, this behavior predicted by the planar tunneling calculations may not hold, but this is beyond the scope of this paper.) The approximations made within the SH theory are valid when $V<0$, because $t(eV,k_\parallel,V,d) \gg t(0,k_\parallel,V,d)$ in this case. However, when $V>0$, the inequality reverses; the holes injected into the base are more populated near E_F ($V \sim 0$), and much less below it. It follows from Eq. (5) that, for $V>0$,

$$\frac{dI_t}{dV} \approx -\frac{e^2}{2}\prod t(0,k_\parallel,V,d) \ . \quad (10)$$

Furthermore, the second term in Eq. (6) becomes small so that the first term can no longer be dropped. Therefore, it is clear from Eqs. (6) and (10), that, in the general case,

$$\frac{dI_c/dV}{dI_t/dV} \neq \tfrac{2}{3}P \quad \text{for } V>0 \ . \quad (11)$$

In this paper, P will be *defined* by Eq. (7) as an experimental quantity. Below we will discuss the TP for the $V>0$ case, but is should be kept in mind that, in this case, P is not proportional to the transmission probability.

C. Free-electron theory of electron-electron scattering

The free-electron theory can be used to obtain an estimate for the inelastic mean free path length λ_i, which is the mean distance that a hot electron will travel before undergoing an e^--e^- collision. This is instructive in allowing comparison to other metals and in providing a framework to discuss the experimental results. We will use the theory of Quinn,[8] who used the Lindhard dielectric constant to derive the imaginary component of the energy, E_I. The lifetime of an excited electron, τ, is related to it by the Heisenberg uncertainty relation. λ_i is defined as the product of τ and the electron group velocity v_g. Assuming a free-electron expression for v_g, Quinn obtained the following result (expressed here in convenient units):

$$\lambda_i \approx \chi \frac{E}{(E-E_F)^2} \ , \quad (12)$$

where

$$\chi = 14.4 \frac{(\beta E_F)^{3/2}}{\tan^{-1}\beta^{-1/2} + \frac{\beta^{1/2}}{1+\beta}} \ . \quad (13)$$

Above, $\beta = \alpha r_s/\pi$, $\alpha = (4/9\pi)^{1/3}$, r_s is the mean distance between electrons in units of the lattice constant of the metal, E is the kinetic energy of the electron, and E_F is the Fermi energy (shown here in units of Å for λ_i, E_F in eV, and E in eV). For $CoSi_2$ band-structure computations[20,21] exist that agree excellently with experimental measurements.[22,23] Reference 23 gives $r_s = 3.95$ and $E_F = 3.21$. Applied to Eq. (13), $\chi = 32.1$. For compar-

ison, corresponding $\{r_s, E_F, \chi\}$ for Au and Al are $\{3.01, 5.53, 46.7\}$ and $\{2.07, 11.7, 79.1\}$, respectively.[24] Figure 1 shows λ_i for Au, Al, and $CoSi_2$ plotted between 0.1 and 6 eV. It can be seen that, based on this theory, $CoSi_2$ is expected to have λ_i 1.45 times smaller than Au and 2.46 times smaller than Al.

A minor improvement on Eq. (12) can be made by keeping v_g explicit. In many metals, the bands near the Fermi level have a linear E-k relation giving a constant group velocity. This is true for $CoSi_2$, which has a nearly linear band Λ_3 along ΓL (parallel to the $\langle 111 \rangle$ direction) extending from 3.41 eV above E_F through E_F.[20] There are two other bands in this energy range along ΓL. One is a Λ_1 band, which is inverted and has a maximum at 0.87 eV, so that it is irrelevant for transport above 0.87 eV from E_F. The other is an electron Λ_1 band that has a minimum at 1.89 eV. Hence it is rigorously correct to associate a single group velocity between 0.87 and 1.89 eV. Therefore, the following equation, obtained from Eq. (12) by keeping v_g explicit, holds rigorously between 0.87 and 1.89 eV, and is an approximation for higher energies up to 3.41 eV:

$$\lambda_i \approx 24.3 \frac{(\beta E_F)^{3/2} E^{1/2} v_g}{\left[\tan^{-1}\beta^{-1/2} + \frac{\beta^{1/2}}{1+\beta}\right](E - E_F)^2} , \tag{14}$$

with v_g in 10^8 cm/s. For the Λ_1 band, $v_g = 0.72$ and Eq. (14) gives

$$\lambda_i \approx 38.7 \frac{E^{1/2}}{(E - E_F)^2} . \tag{15}$$

The above gives a substantially smaller λ_i than Eq. (12), and it is also plotted in Fig. 1 for comparison. For example, at $E = 1$ eV, one gets 79 rather than 135 Å for λ_i. In Sec. IV B 1, a comparison will be made between the above theoretical form and the experimentally measured attenuation length by BEEM for $CoSi_2$/n-type Si(111).

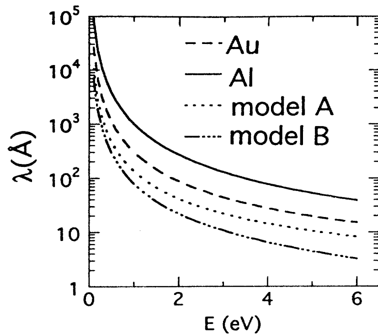

FIG. 1. The inelastic mean free path length λ for $CoSi_2$ (dotted line, model A), predicted by a free-electron theory by Quinn (Ref. 8) was calculated using a band-structure computation of $CoSi_2$ (Ref. 20) and it is shown as a function of electron energy E above E_F. Also shown is λ for $CoSi_2$ (dash-dotted line, model B) resulting from a constant group velocity (0.72×10^8 cm/s) and λ's for Au (dashed line) and Al (solid line).

D. Attenuation length

The attenuation length in BEEM is experimentally a precisely defined number that should be distinguished from the inelastic or elastic mean free path length of hot carriers. To define an attenuation length λ, one assumes that the collector current I_c, under the same tunneling conditions, is an exponential function of the base thickness,

$$I_c(D,E) = I_c(D=0,E) \exp\left[\frac{-D}{\lambda(E)}\right] , \tag{16}$$

where D is the base thickness, and $\lambda(E)$ is the attenuation length at energy E. By comparing BEEM spectra for samples of different thicknesses, one can obtain $\lambda(E)$.

On the other hand, normally the inelastic mean free path length λ_i and the elastic mean free path length λ_e cannot be measured directly by BEEM. These are more fundamental quantities directly related to the lifetimes for inelastic scattering, τ_i, and for elastic scattering, τ_e. In the past, several attempts were made to infer these from BEEM data by performing Monte Carlo simulations.[6,7] In such simulations there are typically a dozen unknown but relevant parameters, e.g., the tip-sample separation, the effect of nonplanar tunneling geometry, λ_e, the degree of $k_\parallel$ conservation at the interface, the degree of backscattering from the substrate by phonon scattering, the specularity of the interface scattering, the specularity of the surface scattering, the momentum distribution of secondary electron-hole pairs generated in the metal, the likelihood of impact ionization in the substrate, the effect of the change of tip-sample separation during the taking of a spectrum, and dynamic transmission effects such as quantum-mechanical reflection.

In our case, there were fewer uncertainties, and we tried to perform BEEM in a way that eliminated as much as possible the effect of the unknown tunnel current distribution, $P(E,k_\parallel)$. For epitaxial $CoSi_2$, there is strong evidence that transport is ballistic within the base in the energy range between the Schottky-barrier height (0.66 eV for n type at 77 K) and a few eV above E_F. Defect scatterings at dislocation cores and point defects in $CoSi_2$ films have been observed with nm resolution by BEEM in this energy range.[9,10,17] This implies that (1) our films have relatively low defect density, (2) multiple-scattering events from the interface and from the surface are not significant, and (3) $P(E,k_\parallel)$ is sharply forward directed. In terms of the hot-carrier lifetime, τ_e exceeds τ_i in this energy range. In this ballistic limit, λ is equal to λ_i averaged over $P(E,k_\parallel)$.

In addition, we use the CH mode of BEEM to minimize the effect of the unknown $P(E,k_\parallel)$. Therefore, the interpretation of our attenuation length is much simpler than was possible for previous studies. For us, $\lambda(E) \sim \lambda_i(E)$, the only significant uncertainty being the angular distribution of injected carriers in the base. This justifies a direct comparison of λ to the theoretical λ_i.

At higher energies the transport becomes diffusive due to the excitation of secondary carriers, rather than by elastic scattering from defects.[12] We now have data for

both forward BEEM of $CoSi_2/n$-type Si(111) and for reverse BEEM of $CoSi_2/p$-type Si(111), which allow a good estimate of the contribution of the secondary carriers to I_c in the high-energy regime. In this regime, λ can become larger than λ_i because the secondary carriers can contribute to the BEEM current and give rise to current multiplication, i.e., a single injected carrier generates multiple carriers (either in the base or in the collector) that may contribute to I_c. Therefore, comparison of λ and λ_i is meaningful only in the low-energy range. (This is estimated to be below ~ 3 eV, by examining the ratio of forward to reverse BEEM current, as explained in Sec. IV B 2.) In Sec. II C, the TP's were discussed. From Eqs. (7) and (16) it follows that

$$P(E)=P_I(E)\exp\left[\frac{-D}{\lambda(E)}\right]. \quad (17)$$

By fitting the TP's as a function of thickness to an exponential form, $\lambda(E)$ can be obtained in the CH-mode BEEM.[10] It should be noted that one should only compare spectra taken with the same tip-sample separation (the same stabilization conditions for V and I_t) and over the same surface structure.

III. EXPERIMENTAL METHOD

Like many metals, carelessly prepared $CoSi_2$ will form polycrystalline thin films or films with pinholes. By using molecular-beam epitaxy (MBE) and carefully controlling growth temperature, deposition rate, annealing time, and annealing temperature, it was possible to grow single-crystalline $CoSi_2$ on Si(111) and Si(100) used for this study. Being single crystalline, these films did *not* have any grain boundaries.

The lattice constant of $CoSi_2$ is smaller than that of Si by 1.2% at room temperature, and $CoSi_2$ has a CaF_2 structure. It is possible to grow relaxed or strained (also called coherent) films of $CoSi_2$ on Si(111) by MBE, and these films have low resistivity [3 $\mu\Omega$ cm at 4 K (Ref. 23)], characteristic of a metal. For our study of $CoSi_2$/Si(111), the layers were grown to be partially relaxed; i.e., misfit dislocations were created in the film to accommodate the lattice mismatch, and the interfacial regions between the dislocations were nearly coherent. For our $CoSi_2/n$-type Si(100), the layers were grown coherently, so that there were no misfit dislocations and the films were lattice matched to the Si(100) substrate by strain.

Our samples were grown using a commercial Si MBE system for 3-in. wafers. The MBE chamber was connected to a STM chamber, and a home-built STM was used to investigate *in situ* the samples grown by MBE. The base pressure of our MBE chamber was $\sim 10^{-11}$ mbar, and the pressure during growth remained below $\sim 10^{-9}$ mbar. The STM was especially made to examine 3-in. wafers at 77 K for microscopy (STM) and also for ballistic-electron-emission microscopy (BEEM).[25] The tungsten STM tips were prepared by chemical etching and cleaned by *in situ* Ar-ion bombardment. The MBE chamber was also connected to a commercial plasma chamber capable of hydrogen etching SiO_2.[26]

In order to obtain Ohmic contacts to the substrates, only degenerately doped Si substrates were used. The Si wafers used for our MBE growth had unintentional misorientations of less than 0.3°. Prior to the silicide growth, the wafers were first outgassed at 500 °C for ~ 2 h and then at 700 °C for $\sim \frac{1}{2}$ h. For most samples, the wafers were then ramped to 840 °C, exposed to a weak Si flux (less than ~ 0.5 Å/s) to remove residual SiO_2, and then 3000–10000-Å-thick undoped Si buffer layers were grown at 700 °C. For some wafers, plasma etching was used for oxide removal[26] prior to the buffer growth. As characterized by BEEM, there was no unambiguous difference between samples prepared with and without plasma etching.

For p-type wafers, boron segregation during the 840 °C oxide removal step caused an increase in Si buffer defect density and consequently lowered the quality of the silicide films. Two methods were found to solve this problem. In the first, plasma etching was done without a process going over 700 °C. In the second, one monolayer of Si was deposited at 840 °C and then 100 Å of Si were deposited at 400 °C, followed by annealing for ~ 30 min at 600 °C. After both of these, 7×7 surface reconstruction could be seen by reflection high-energy electron diffraction (RHEED), and a good quality Si buffer could be grown on top.

For growth on Si(111), thin films of $CoSi_2$ were made by stoichiometric codeposition of Co and Si onto the 7×7 Si(111) surface at room temperature followed by a monolayer of Si-capping layer and annealing at 600 °C for 2–10 min. The excellent quality of the preparation of the 7×7 Si(111) surface has been previously confirmed by our group in *in situ* STM and RHEED studies.[27] For the present case, the same preparation was done.

The deposition rates were monitored by two quartz-crystal-thickness monitors. The thickness calibration was done by growing a layer of nominal thickness then measuring it *ex situ* by Rutherford-backscattering spectrometry or by weighing. In the latter method, knowing the density of $CoSi_2$ and the weight of the wafer before the deposition, the deposited film thickness could be calculated with less than $\sim 10\%$ error.

The procedure for silicide growth described above is known to produce pinhole-free $CoSi_2$, consisting of atomically smooth interfacial regions bounded by misfit dislocations.[27] The partially relaxed $CoSi_2$ is found to contain a nearly hexagonal network of misfit dislocations, which are always associated with steps at the $CoSi_2$/Si interface.[28] Hence neighboring $CoSi_2$ regions, separated by a dislocation, *always* differ in thickness by one or two atomic layers, but appear flat on the surface, except for small protrusions (< 1 Å, and having a Lorentzian profile) near the dislocation, due to the elastic deformations around its core.[29–31] Hence it is possible unambiguously to identify interfacial steps in topographic STM images.[30] The surface was mostly 1×1, except in very thin layers where some areas of strain-induced 2×1 reconstruction could be seen.

The growth on Si(100) was done using a template method.[32] For a typical sample, first 1.6–2 Å of Co was deposited onto 2×1 Si(100) followed by codeposition of

5–7 Å of silicide with a stoichiometry of $CoSi_{1.6}$-$CoSi_{1.8}$ at room temperature. This template was then annealed for ~2 min at 350 °C and allowed to cool to room temperature. Then additional silicide with the same stoichiometry was deposited, and a few monolayers of Si cap were also deposited to create a film of the desired thickness. This film was finally annealed at 600 °C for 2–10 min. As for $CoSi_2$/Si(111), the $CoSi_2$/Si(100) films grown by the template technique were single crystalline and without pinholes (confirmed by a detailed study reported in Ref. 32). However, since our $CoSi_2$/Si(100) samples were thinner than the critical thickness for the onset of misfit dislocations (~100 Å), the 30–50-Å-thick samples used for this study were strained (coherent).

IV. RESULTS AND DISCUSSION

A. Interfacial transmission probabilities

1. *$CoSi_2$/n-type Si(111) vs $CoSi_2$/p-type Si(111)*

It is fairly well established that, in the absence of scattering, the tunneling electron distribution $P(E,k_{\parallel})$ between planar electrodes[33] or from the STM tip to the metal surface[34] is sharply forward directed. In other words, the tunneling electrons have small $k_{\parallel}$. If $k_{\parallel}$ conservation held across the *m-s* interface, then this together with energy conservation would impose a severe kinematic constraint on I_c, especially for semiconductors with conduction-band minima away from the zone center. This was originally pointed out by Schowalter and Lee,[7] who also demonstrated that $k_{\parallel}$ conservation must not hold for Au/Si, because $I_c(E)$ is nearly identical for Au/Si(100) and Au/Si(111). A more recent study also confirmed this experimental finding.[35] Scattering in Au (Refs. 7, 16, and 35) or at the Au/Si interface[16] was presumed to cause this.

However, unlike Au/Si, it is known that the interface of epitaxial $CoSi_2$/Si is atomically abrupt and that translational invariance is preserved along most of the interface (except at misfit dislocations and point defects), so that one would expect at least a partial conservation of $k_{\parallel}$. For Au on *n*-type Si(111), it was pointed out that elastic scattering should tend to increase I_c, by providing the $k_{\parallel}$ necessary to match the $k_{\parallel}$ of the Si conduction band projected on the interface.[7] We have observed that, indeed, elastic scattering at the misfit dislocation core does increase the BEEM current for $CoSi_2$/Si(111).[9] Furthermore, a typical BEEM image showed many small regions of higher I_c which are associated with localized point defects in the $CoSi_2$ film. However, it was not clear if the absolute magnitude or the spectral shape were as predicted by the BK theory.

In principle, additional confirmation of $k_{\parallel}$ conservation can be made with help from $CoSi_2$/*p*-type Si(111), which has *exactly* the same surface and interface structure as $CoSi_2$/*n*-type Si(111). For the *p*-type substrate, the final state in Si is a zone-centered valence band which projects near the interface Brillouin-zone center. This implies that, if $k_{\parallel}$ conservation held at this interface, (1) elastic scattering should decrease I_c and (2) the transmission probability across the interface should be much larger for the *p* type than the *n* type substrates. However, the unknown dynamic transmission effects at this interface may be significant. They were calculated to give approximately a factor of 3 difference in ITP for type-A and type-B $NiSi_2$/Si(111).[11]

In Fig. 2, two representative averaged TP's for a 30-Å-thick $CoSi_2$/*n*-type Si(111) film and for a 30-Å-thick $CoSi_2$/*p*-type Si(111) film are shown. The derivatives used to compute the TP's were extracted numerically. Linear least-square fits (LSF's) were done to examine the threshold behaviors, and these are shown with the data. For $CoSi_2$/*n*-type Si(111), the linear fit gives an energy-axis intercept of 0.72 eV, which agrees well with the expected Schottky barrier height of 0.66 eV within the experimental error, which is estimated to be 1–2 times the data spacing and comes from the numerical differentiation used to obtain the TP's. The numerical differentiation was done by doing a LSF to a quadratic

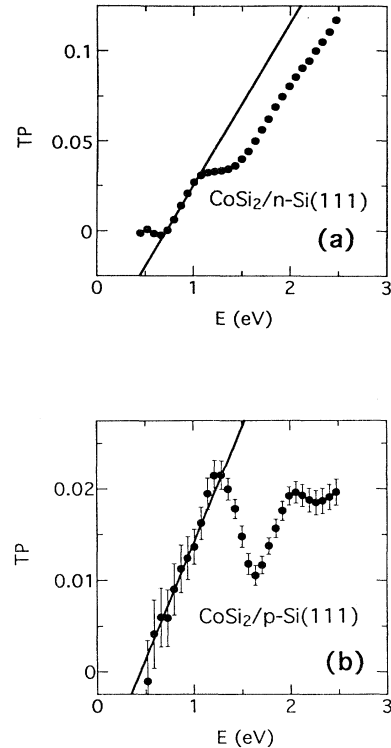

FIG. 2. (a) An average of ~2000 transmission probabilities (TP's) for a 30-Å-thick $CoSi_2$/*n*-type Si(111) film taken in the CH-mode BEEM. The data were taken every 70 mV, and the stabilization condition was $V=-0.6$ V and $I_t=0.2$ nA. A least-square fit (LSF) gave the linear line drawn through the threshold region. It has an energy-axis intercept of 0.72 eV and a slope of 0.090/V. (b) An average of ~2000 TP's for the 30-Å-thick $CoSi_2$/*p*-type Si(111) film. In this case, a LSF gave the displayed line that has an energy-axis intercept of 0.45 eV and a slope of 0.025/V. The data were taken every 70 mV, and the stabilization condition was the same as in (a).

equation using two points on both sides of each data point. An effective smoothing is thus done, and it gives a conservative error estimate. The slope of the fit line is 0.090/V. For the case of $CoSi_2$/*p*-type Si(111) shown in Fig. 2(b), the linear line through the data has an energy-axis intercept of 0.45 eV, which agrees with the expected value of 0.51 eV (Schottky-barrier height) within the experimental error, and the line has a slope of 0.025/V. The ratio of the slopes is 3.5. Not only is the TP smaller rather than larger, as expected by purely kinematic considerations, but it is substantially smaller.

For the most part, this anomaly may be due to a breakdown of the approximations in the theory for CH-mode BEEM when the tip-sample bias is positive, which was demonstrated in Sec. II B. The effect of $P(E,k_{\parallel})$ will be discussed further in Sec. IV A 3.

Away from the threshold, the spectral shapes are nonlinear in both cases. For the *n*-type substrate, there is a roll-off near the band-gap energy of Si at ~ 1.2 eV, and an additional threshold at ~ 1.8 eV. The roll-off has been previously assigned to electron-hole pair creation at the metallurgical interface[10,16] and the high-energy threshold to transport into L_1 of the Si conduction band.[9]

The averaged spectrum for the *p*-type substrate also exhibits a roll-off at ~ 1.2 eV. Higher-energy features cannot be unambiguously identified due to the effect of $P(E,k_{\parallel})$.

2. $CoSi_2$/n-type Si(111) vs $CoSi_2$/n-type Si(100)

Within the purely kinematic BK theory,[1] I_c for Au/Si(100) should be more than an order of magnitude larger than for Au/Si(111).[7] For $CoSi_2$/Si, this is not certain, because the surface structures are quite different for $CoSi_2$/Si(100) and $CoSi_2$/Si(111). It has been shown previously that surface reconstructions can significantly change I_c.[25] Whereas most of the $CoSi_2$/Si(111) surfaces are unreconstructed, the $CoSi_2$/Si(100) surface always displays surface reconstructions, the dominant one being $3\sqrt{2}\times\sqrt{2}R45°$ and sometimes $\sqrt{2}\times\sqrt{2}R45°$ also appearing (we will omit $R45°$ from here for brevity).

In Fig. 3 we show an average of TP's taken over a region of $CoSi_2$/Si(100) that was atomically resolved to be $3\sqrt{2}\times\sqrt{2}$. The base thickness was 30 Å and the tip-stabilization condition was the same as for Fig. 2. A least-square fit (LSF) gave the displayed line, which has a energy-axis intercept of 0.68 eV and a slope of 0.20/V. In comparing the slope here to that of $CoSi_2$/Si(111), one finds a TP that is 2.2 times larger. It will be shown in Sec. IV B 1 that λ for $CoSi_2$/Si(100) is ~ 2.0 times shorter (at 1.5 eV) than for $CoSi_2$/Si(111). Thus, in the zero thickness limit, the ratio of TP's are expected to be ~ 4 times larger.

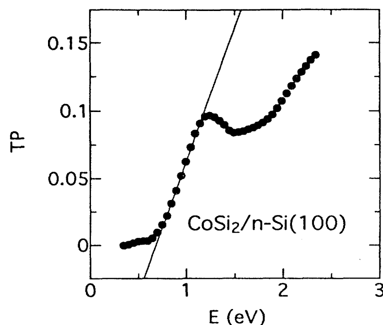

FIG. 3. An average of $\sim$2000 TP's for a 30-Å-thick $3\sqrt{2}\times\sqrt{2}$-surface-reconstructed $CoSi_2$/*n*-type Si(100) taken with a tip-stabilization condition of -0.6 V and 0.2 nA. A least-square fit gave the displayed line that has an energy-axis intercept of 0.68 eV and a slope of 0.20/V. The data were taken every 50 mV.

It is possible that interfacial scattering may play some role. Whereas $CoSi_2$/Si(111) is known to have eightfold-coordinated Co atoms everywhere, with Si being bulk terminated at the interface,[28] two interfacial models were proposed for $CoSi_2$/Si(100). In one, Co atoms at the interface are sixfold coordinated and interfacial Si atoms preserve their bulk tetrahedral bonding geometry and lengths. In the other model, the interfacial Si atoms form a 2×1 reconstruction.[36] We do see at least two types of interfaces. In Fig. 4(a) we show two TP's (averages of $\sim$2000 each) taken over two $3\sqrt{2}\times\sqrt{2}$ regions (confirmed by atomic-resolution STM) lying next to each other, and in Fig. 4(b) we show CC-mode spectra taken over the same regions along with a difference spectrum. The error bars do not show simple correlation with the magnitude of I_c, and this may be partially due to the error being real spatial variation of I_c, which can have an energy dependence; for example, scattering from a dislocation depends on energy.[9] The sample was a 50-Å-thick $CoSi_2$/Si(100) film. There is no surface step separating the two regions. In both modes of BEEM, the spectra can be seen to cross at a certain voltage. The value of the voltage is different between the CH-mode and CC-mode spectra, but this may be expected from the difference in the two techniques. It was shown in Ref. 10 that CC-mode spectra and CH-mode spectra can be quite different at high bias due to effects in the tunnel gap. However, even in the CC mode, the spectra are reproducible, and there exist many regions with essentially the same spectra. The crossing of the spectra cannot be explained by a thickness effect,[12] which is expected to be dominant at high energies and is expected to increase monotonically as a function of energy. Quantum-size effects (QSE's) for $CoSi_2$/Si(100) are expected to be relatively weak in comparison to $CoSi_2$/Si(111), since Si has no gap (from ~ 0.7 eV above E_F to much higher energies) in the $\langle 100 \rangle$ direction to allow the formation of bound one-dimensional (1D) states in $CoSi_2$ along ΓX, and ubiquitous surface reconstructions would broaden any weak resonances in the films. Even though we observed strong QSE's for $CoSi_2$/Si(111) by current-imaging-tunneling spectroscopy and modulation spectroscopy,[12,17] until now we have not observed any for $CoSi_2$/Si(100) by the same techniques. Therefore, we are led to conclude that there must exist at least two types of interfacial structures for $CoSi_2$/Si(100).

3. *Effect of tunnel current distribution*

The development of CH-mode BEEM was motivated by the need to eliminate the effect of the unknown tunnel

current distribution, $P(E,k_{\parallel})$, as much as possible.[11] It was demonstrated[10] to give a very different high-energy spectrum from CC-mode BEEM, in which the tunnel current is always kept constant by adjusting the tip-sample separation. At high energies, peaks in the CC-mode BEEM spectra appeared where the CH-mode spectra were nearly featureless.

Another example of the importance of $P(E,k_{\parallel})$ for BEEM can be seen in forward BEEM of $CoSi_2/p$-type Si(111), in which the tip voltage is biased positively with respect to the sample. $P(E,k_{\parallel})$ is *always* peaked near the cathode's Fermi level because the electrons with the highest energies are most likely to tunnel across the vacuum barrier. In p-type forward BEEM, only the low-energy tail of $P(E,k_{\parallel})$ can contribute to the BEEM current,[37] so that, in the CC mode, I_c in forward BEEM of $CoSi_2/p$-type Si(111) is expected to be much smaller than the I_c in forward BEEM of $CoSi_2/n$-type Si(111). In Fig. 5, a pair of CC-mode BEEM spectra are shown to compare the relative magnitudes of the forward BEEM currents between a 22-Å-thick $CoSi_2/p$-type Si(111) film and a 22-Å-thick $CoSi_2/n$-type Si(111) film. While the latter tends to increase monotonically, the first reaches a maximum at $\sim 3|V|$ then decreases. If one ignores unexpected pathological transmission probabilities into the Si valence band, the roll-over of the spectrum must be due to the sharpening of the energy distribution of the tunneling electrons at high bias (CC-mode BEEM), which makes fewer electrons available at its tail to contribute to I_c in forward BEEM of $CoSi_2/p$-type Si(111).

The CH mode may eliminate some of the dependence on $P(E,k_{\parallel})$. However, even for the normal case when STM injects electrons into the base, the tip-stabilization condition (effectively the same as the tip-sample separation, d) for the CH-mode BEEM may be important. For an ideal interface where subtle dynamic and kinematic effects can be seen, the TP was predicted to be sensitive to d. Figure 6 shows three TP's taken for three different tip-stabilization conditions over the same area on a 72-Å-thick $CoSi_2/n$-type Si(111) film. Even though the tip-stabilization voltage took on values of -0.2, -0.6, and -0.9 V, the actual d should have changed by less than an Å. d was not measured in this case ($I_t=0.2$ nA), but the statement was found to be true when $I_t=1$ nA. There is a tendency at high bias for TP's stabilized at larger d's (corresponding to larger V's) to be larger, and this may be due to a breakdown of the assumptions of SH theory at higher voltage.[11] At low energies, the two TP's stabilized at -0.6 and -0.9 V are nearly identical, but the one at -0.2 V is substantially smaller. However, scaling it by a factor of 1.3 makes it similar to the others. It can be concluded that the TP does depend on d, as expected. However, it should be noted that, while in theory one can change d by dozens of Å at will, in practice one

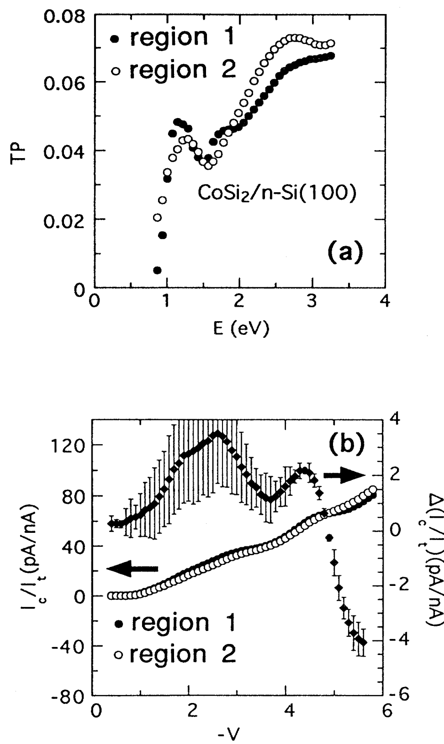

FIG. 4. Over two side-by-side regions on a 50-Å-thick $3\sqrt{2}\times\sqrt{2}$-surface-reconstructed $CoSi_2/n$-type Si(100) (confirmed by atomic-resolution STM), CH-mode BEEM and CC-mode BEEM were performed. There is no surface step separating the two regions. (a) For each region, ~2000 TP's were averaged. Region 1 (filled circles) shows a larger TP than region 2 (unfilled circles) at low energies, but a smaller TP at high energies. The tip stabilization was at -0.6 V and 0.2 nA, and the data were taken every 70 mV. (b) Two averages of ~600 spectra each show BEEM current I_c/I_t (taken in the CC mode) for regions 1 (filled circles) and 2 (unfilled circles). The difference spectrum is also shown with error bars calculated from error bars for each spectrum. A pure thickness effect would always make one spectrum larger than the other. Therefore, regions 1 and 2 must have different interfacial structures. The crossover points in (a) and (b) are different, and this is attributed to differences between CC-mode and CH-mode BEEM, as explained in the text.

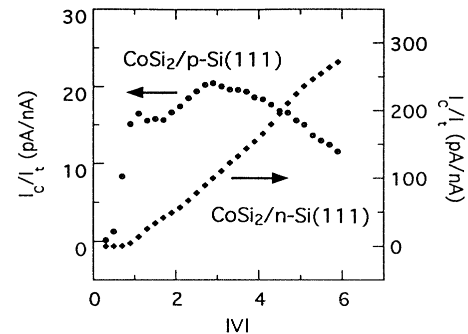

FIG. 5. A pair of CC-mode BEEM spectra is shown to compare the relative magnitudes of the forward BEEM currents between a 22-Å-thick $CoSi_2/n$-type Si(111) film (diamonds) and a 22-Å-thick $CoSi_2/p$-type Si(111) film (filled circles). In the latter case, the BEEM current I_c/I_t is strongly shaped by the asymmetry of the tunnel current distribution.

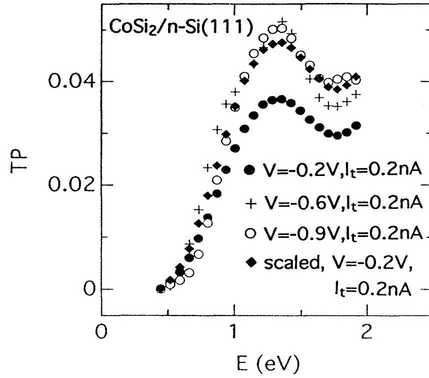

FIG. 6. The TP's (averages of ~2000 each) for three different tip-stabilization conditions (corresponding to three different tip-sample separations, d's) over the same area on a 72-Å-thick $CoSi_2$/Si(111) film. The tip-stabilization conditions were $V=-0.2$ V and $I_t=0.2$ nA (filled circles), -0.6 V and 0.2 nA (+'s), and -0.9 V and 0.2 nA (open circles). For low energies, the latter two are the same within the uncertainty in the TP's (not shown, but approximately a few percent of a TP). The first TP is substantially smaller, but it has the same shape as the others. When multiplied by 1.3 (shown in diamonds), it converges with the other two.

cannot change it too much without leaving the range of detectable signals, either by obtaining values of I_t and I_c that are too large or too small during the taking of a spectrum.

B. Hot-electron–electron scattering in $CoSi_2$

1. Comparison between (111) and (100)

For our attenuation length study of $CoSi_2/n$-type Si(111) using CH-mode BEEM, relaxed samples of thicknesses 25, 30, and 72 Å were used. For CC-mode BEEM, samples of 30, 42, and 72 Å were used. The relaxed samples had mostly unreconstructed surfaces. Due to a systematic error in the thickness calibration, it is estimated that there is a ~10% systematic error in our measured λ's.

In Fig. 7(a) we show λ (in Å) obtained from the CH mode for $CoSi_2/n$-type Si(111) along with a best-fit line of the form

$$\lambda \approx a + b(E-E_F) + \frac{cE^{1/2}}{(E-E_F)^2}, \tag{18}$$

where $a=39.5$, $b=-3.17$, and $c=19.2$. The above is a phenomenological equation inspired by Eq. (15) of the free-electron theory. The fit was done to give a convenient and accurate description of data that can be used for comparison with other data.

The error bars shown in Fig. 7(a) are uncertainties from the least-square fits (LSF's) done to obtain λ. Because the TP's are ratios of derivatives, they are susceptible to noise. Also shown is the theoretical λ given in Eq. (15), which was computed using band-structure parameters from Ref. 20 and Quinn's theory.[8] A clear disagreement of the free-electron theory and the data can be seen for the entire range, including the range below 3 eV where electron transport through the base is expected to be ballistic. (See Sec. IV B 2 for a discussion on the transition to the diffusive regime. In the diffusive regime, λ's measured by BEEM overestimate the true λ because of the contribution from secondary electrons created in the base.) This is hardly surprising because $CoSi_2$ consists of three-nested hole sheets at the Fermi surface, and hence it is not expected to behave like a free-electron metal.

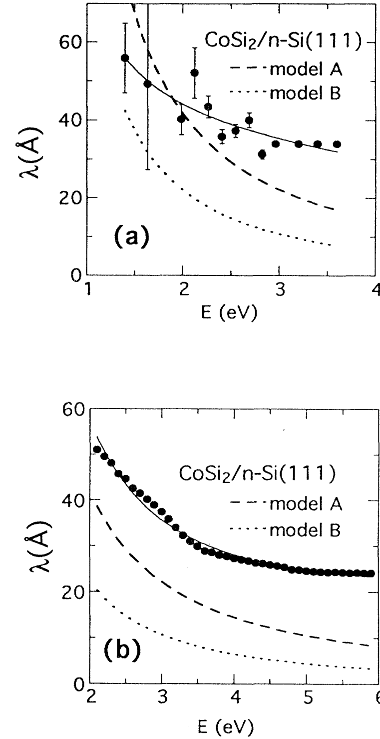

FIG. 7. (a) The attenuation length λ measured by CH-mode BEEM on $CoSi_2/n$-type Si(111) is shown along with the predicted inelastic mean free path length λ_i's, by Quinn's free-electron theory [model A, dashed line, Eq. (12) of the text] and by a modified free-electron theory [model B, dotted line, Eq. (15) of the text]. Also, a fit (solid line) through the data using a phenomenological form [Eq. (18) of the text] is shown. The discrepancy between the free-electron theory and the data is evident. For the data, three samples of thicknesses 25, 30, and 72 Å were used. For each sample, ~2000 CH-mode BEEM spectra were taken over arbitrary locations. For *all* CH-mode BEEM, the initial stabilization condition was the same in order to obtain a constant tip-sample separation; the tip was stabilized at $V=-0.6$ V and $I_t=0.2$ nA before the STM feedback loop was interrupted for the taking of a CH-mode spectrum. (b) The same measured by CC-mode BEEM. For each sample, ~2000 CC-mode BEEM spectra were taken over arbitrary locations. Below ~2 eV, quantum-size effects distorted the spectra and hence it was difficult to determine λ. $\lambda(E)$ at high energies ceases to decrease, and becomes nearly constant, due to the increasing contribution of secondary electrons to I_c. In that regime, $\lambda \neq \lambda_i$ and the transport is diffusive rather than ballistic. Also shown is a phenomenological fit to Eq. (18).

Furthermore, low-energy optical interband transitions are allowed to occur ($\Delta_5 \rightarrow \Delta_1$ at $\sim$0.3 eV and $\Sigma_1 \rightarrow \Sigma_3$ at $\sim$0.5 eV), and may have been seen.[38] The phase space for electronic interband transitions is expected to be larger, so these are expected in $CoSi_2$/Si(111) even at energies below the Schottky-barrier height. Interband transitions should make the λ even shorter.[39]

In Fig. 7(b) we show λ obtained in the CC mode and fit to the same function. They both show a monotonic decrease with energy up to 4 eV, and fit well to the same function shown in Eq. (18) but with parameters that are quantitatively very different: $a=12.2$, $b=0.762$, and $c=76.6$ in this case. Only λ's above 2 eV are shown, because, below, quantum-size effects affected the spectra. Energy-dependent QSE's in $CoSi_2/n$-type Si(111) were previously reported.[12] The high-energy portion of λ is shown to illustrate that it ceases to decrease at high energies and becomes nearly constant. This is due to the contribution of secondary electrons to I_c at high energies.

λ's for $CoSi_2/n$-type Si(100) taken in the CH and CC modes are shown in Fig. 8(a). Also shown is a fit to Eq. (18) with $a=17.6$, $b=2.16$, and $c=3.89$. For the CC-mode measurement, samples of thicknesses of 30, 38, and 50 Å were used, while for the CH mode thicknesses were 30 and 50 Å. To ensure that surface effects did not play a dominant role, atomic-resolution STM was performed, and the spectra taken only over $3\sqrt{2}\times\sqrt{2}$-reconstructed areas. The spectra over two kinds of interfacial structures (explained in Sec. IV A 2) were weighed equally and averaged. In Fig. 8(a), λ is seen to be substantially smaller than λ for $CoSi_2/n$-type Si(111), the ratio being $\sim$0.5 at 1.5 eV. The error bars were calculated from errors of the TP's used.

Similar λ, obtained from CC-mode BEEM spectra, can be seen in Fig. 8(a). Spectra for 30- and 50-Å-thick films were taken from exactly the same location as for the CH-mode spectra. To obtain λ, $\ln(I_c)$ for 30, 38, and 50 Å were plotted on a linear scale, and linear LSF's were performed, as shown in Fig. 8(b). The reciprocals of the slopes were taken as λ's, and the errors associated with the fits were assigned as the error bars shown. It can be seen in Fig. 8(b) that Eq. (16) (assuming the exponential dependence of I_c on D) is a good assumption. The CC-mode λ should not be taken to be precise, since it can be affected by a change of the unknown $P(E,k_{\parallel})$. However, λ from the CC-mode spectra supports the noisier λ from the CH-mode spectra.

Therefore, both CH-mode and CC-mode BEEM showed that λ for $CoSi_2/n$-type Si(100) is significantly smaller than λ for $CoSi_2/n$-type Si(111). It is possible that the difference is partially caused by a wider angular distribution of electrons under the $3\sqrt{2}\times\sqrt{2}$-reconstructed surface. It could also be a band-structure effect. For $CoSi_2/n$-type Si(100), there is a $\Delta_{2'}$ band between 0.79 and 1.57 eV with relatively low group velocities, and there are two other bands (Δ_1 and Δ_5) in the same energy range that could participate in interband scattering.[20] In any case, in the ballistic transport regime below 3 eV, the shape and magnitude of λ differ strongly from predictions of the free-electron theory shown in Figs. 1 and 7(a).

2. *Spatial distribution of hot carriers*

At higher biases, electrons injected into the sample by the STM tip have enough energy to either excite electron-hole pairs in the base[13] or in the semiconductor,[6] giving rise to secondary carriers that can increase the BEEM current. There are many works dealing with impact ionization in the semiconductor.[40]

The BEEM current does become large at high biases. To determine whether this is due mostly to charge multiplication in the base or to impact ionization, or to nei-

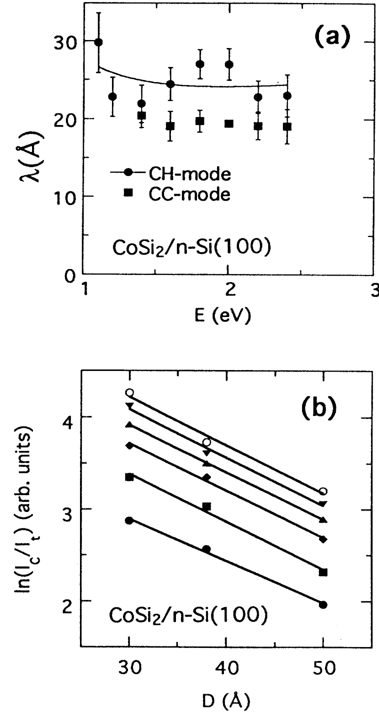

FIG. 8. (a) The attenuation lengths λ's measured by CH-mode and CC-mode BEEM on $CoSi_2/n$-type Si(100) are shown. The stabilization parameters were the same as for $CoSi_2/n$-Si(111) (-0.6 V and 0.2 nA), and about $\sim$2000 spectra taken were averaged. Also, a fit (solid line) through the CH-mode data using a phenomenological form [Eq. (18) of the text] is shown. Two samples of thicknesses 30 and 50 Å were used for the CH-mode data. The spectra over two kinds of interfacial structures (explained in Sec. IV A 2) were weighed equally and averaged. For the CC-mode data, three samples of thicknesses 30, 38, and 50 Å were used. The error bars shown were derived from uncertainty in the least-square fits (LSF's) shown in (b). For the 30- and 50-Å-thick films, the CH-mode and CC-mode data were taken consecutively over the same regions, and the same weighing and averaging were performed. It can be seen that the λ shown is very different in both magnitude and shape from the λ for $CoSi_2/n$-type Si(111). (b) To calculate the CH-mode λ's shown in (a), $\ln(I_c/I_t)$ for the three thicknesses were plotted in a log-linear scale and LSF lines were fit, as shown here. The reciprocal of the slopes gave the λ's. It can be seen that, to a good approximation, I_c/I_t is an exponential function of the base thickness D for the energy range between 1.4 and 2.4 eV above E_F. The lower fit lines correspond to smaller E's.

ther, one should first consider the spatial resolution of BEEM. Previously, it was shown that atomic thickness variations in the base can be detected by BEEM imaging. If impact ionization from primary electrons (those injected by the STM tip that did not undergo any inelastic collision in the base) dominates, then a BEEM image at high bias should show nm-scale thickness contrasts. The reader should note that we observe nm-scale resolution in low-bias BEEM of $CoSi_2$/n-type Si(111),[9,10,25] and that, at high bias, the tunnel current distribution becomes more sharply focused because the tip-sample separation increases in order to maintain the same I_t. Hence, neglecting the contribution to I_c from the base, the spatial resolution of BEEM should only become better at high bias. However, should the contribution to I_c from secondaries be significant, then the resolution (of interfacial objects) will directly reflect the spatial distribution of the secondaries in the base, which is expected to be diffusive. The net BEEM current will be a sum of the primary current with nm resolution and secondary current with much worse resolution. Degraded resolution for high-bias forward BEEM has been observed previously.[12]

Figures 9(a) and 9(b) show a pair of simultaneously taken STM and forward BEEM images of a 22-Å-thick $CoSi_2$/n-type Si(111) film. The STM image is an empty-state image showing three monolayer steps each 3.1 Å high and a nearly hexagonal network of faint lines due to strain fields surrounding misfit dislocations. The BEEM image shows nearly discrete contrasts due to atomic thickness variations of the base. Thinner areas of the base transmit more electrons and hence appear lighter in the BEEM image.

An arbitrary line section has been taken from the image, and has been fit to an erf function defined as below in

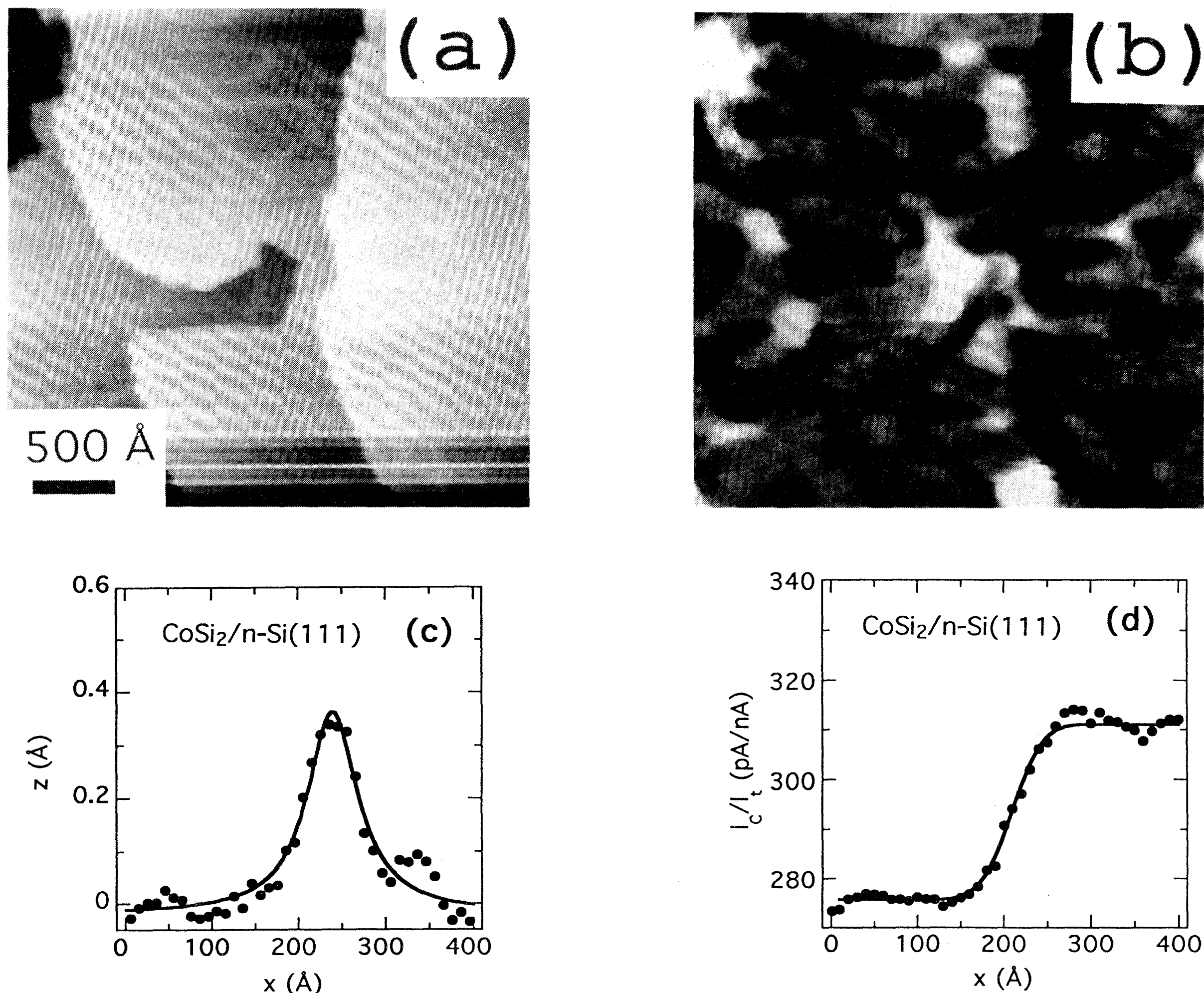

FIG. 9. (a) and (b) are a pair of simultaneously taken STM and forward BEEM images of a 22-Å $CoSi_2$/n-type Si(111) film over a 3000×3000-Å^2 area. Empty states were probed and $V=-6$ V and $I_t=2$ nA. The STM image shows three monolayer steps each 3.1 Å high, and a strain field due to dislocation appearing as a light network. The BEEM image shows atomic thickness variations of the film. The gray scale in the BEEM image is from 467 (black) to 736 pA (white). Areas appearing darker are thicker areas. (c) and (d) are an arbitrary pair of STM and BEEM line sections taken from the area shown in (a). The topography profile was fit to a Lorentzian, and the BEEM profile was fit to an erf function as described in the text.

order to quantify the resolution:

$$I_c = I_0 + \frac{\Delta I}{\sqrt{\pi}} \int_{-\infty}^{x} \exp\left[-\frac{(u-x_0)^2}{\delta^2}\right] du \ , \qquad (19)$$

where I_0 is the lower BEEM current, ΔI is the current difference away from the thickness contrast, and the thickness is assumed to change at x_0 and to be larger on the positive-x side. In Figs. 9(c) and 9(d) we show the topographic line section fit to a Lorentzian (the FWHM is 35 Å, the height is 0.38 Å, and the section is centered at 240 Å), and a corresponding BEEM section with a fit to Eq. (19). For the fit shown, $\delta=40$ Å (centered at 209 Å), and the fit is excellent. However, some BEEM line sections deviate slightly from the erf function form. It is more appropriate to define a more robust spatial resolution R of BEEM as the distance over which the BEEM current changes from 10% to 90% of its final value. For an erf function, $R=1.81\delta$, so that R in Fig. 9 is 72 Å. From ten cross sections of the image shown in Fig. 9(a), an R of 76 ± 20 was obtained for forward BEEM of 22-Å-thick $CoSi_2/n$-type Si(111) at -6 V.

If one performs reverse BEEM on p-type Si, then the tip-sample bias is negative, so that the tunnel current distribution is exactly the same as for forward BEEM on n-type Si, and hence almost exactly the same processes should occur in the base and in the semiconductor. One important difference is that, for p-type(n-type)Si, only holes (electrons) are collected, and that the transmission probability for electrons and holes differs. At a few eV above the Schottky barrier, ITP's for both electrons and holes are expected to approach unity, and hence it should be a good approximation to assume equal ITP's for high-energy electrons and holes. In addition, we assume that the distribution of the secondary electrons and holes are approximately the same. Then reverse BEEM on p-type Si (collecting only secondary holes) allows one to obtain a good estimate of the secondary current for the forward BEEM on n-type Si (collecting only electrons). Figure 10 shows a pair of CC-mode BEEM spectra to compare forward BEEM on n-type Si and reverse BEEM on p-type Si, both for 22 Å $CoSi_2$/Si(111). It can be estimated that at 6 V, $\sim\frac{2}{3}$ of the contribution to I_c comes from secondary electrons. At ~ 3.7 V, I_c for p-type Si becomes 50% of I_c for n-type Si. Under the assumptions we stated above, we may define energies above ~ 3 V as a high-energy regime where the contribution from the secondary carriers begins to dominate I_c.

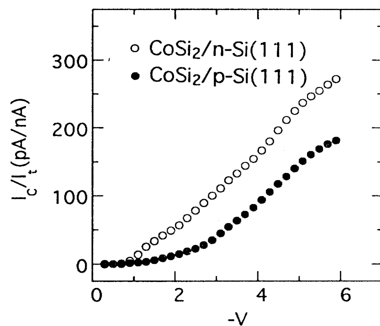

FIG. 10. A pair of CC-mode BEEM spectra are shown to compare a forward BEEM spectrum on a 22-Å-thick $CoSi_2/n$-Si(111) film (unfilled circles) to a reverse BEEM spectrum on a 22-Å-thick $CoSi_2/p$-type Si(111) film (filled circles). In both cases, the tunnel current distribution should be exactly the same. However, in the forward BEEM case, primary and secondary electrons are collected while, in the reverse BEEM case, only secondary holes are collected.

If one examines a high-bias reverse BEEM image, then one should obtain a slightly worse spatial resolution due to the absence of primary current, but should still see mostly the same features as the high-bias forward BEEM image, since in both cases secondaries generated in the base dominate. Figures 11(a) and 11(b) show a pair of simultaneously taken STM and reverse BEEM images of a 22-Å-thick $CoSi_2/p$-type Si(111) film. The STM image is an empty-state image, the gray scale ranging over 7.46 Å. As for Fig. 9, atomic thickness variations show up as nearly discrete contrasts in the BEEM image. However, due to the opposite polarity of holes, thinner regions transmit more reverse BEEM current and appear darker in Fig. 11(b). In Figs. 11(c) and 11(d) we show arbitrarily taken line sections from Figs. 11(a) and 11(b). The topography section is again fit to a Lorentzian (the FWHM is 35 Å, the height is 0.47 Å, and the section is centered at 194 Å), and the BEEM profile is fit to Eq. (19). For the fit shown, $\delta=55$ Å ($R=100$ Å, and is centered at 198 Å) and the fit is excellent. Taking ten random line sections from the image and defining the spatial resolution as before, an R of 106 ± 22 is obtained, in fulfillment with our expectations.

V. SUMMARY

Ballistic-emission microscopy was performed to study hot-carrier transport in epitaxial films of $CoSi_2$ on Si(111) and Si(100). The attenuation length λ in the ⟨100⟩ direction for $CoSi_2/n$-type Si(100) has been measured by both CH-mode BEEM and conventional CC-mode BEEM, and its was found to be significantly smaller than the λ in the ⟨111⟩ direction on $CoSi_2/n$-type Si(111), the ratio of the λ's being ~ 0.5 at 1.5 eV above Fermi energy. For both directions, the λ's were found to behave very differently from predictions of a free-electron theory.

As the energy of the injected carries was increased, a transition from ballistic transport in the metal overlayer to a diffusive transport was observed, with an accompanying significant degradation of the spatial resolution of both forward and reverse BEEM, which implied that the dominant contribution to the BEEM current must originate from the base. A comparison of forward BEEM on $CoSi_2/n$-type Si(111) and reverse BEEM on $CoSi_2/p$-type Si(111) allowed an estimate of primary and secondary BEEM current contributions.

Constant-height-mode BEEM was used to investigate the transport across these interfaces. For a 30-Å-thick film, the TP near the Schottky-barrier threshold for $CoSi_2/n$-type Si(100) was ~ 2.2 times larger than for a $CoSi_2$ film of the same thickness grown on n-type Si(111).

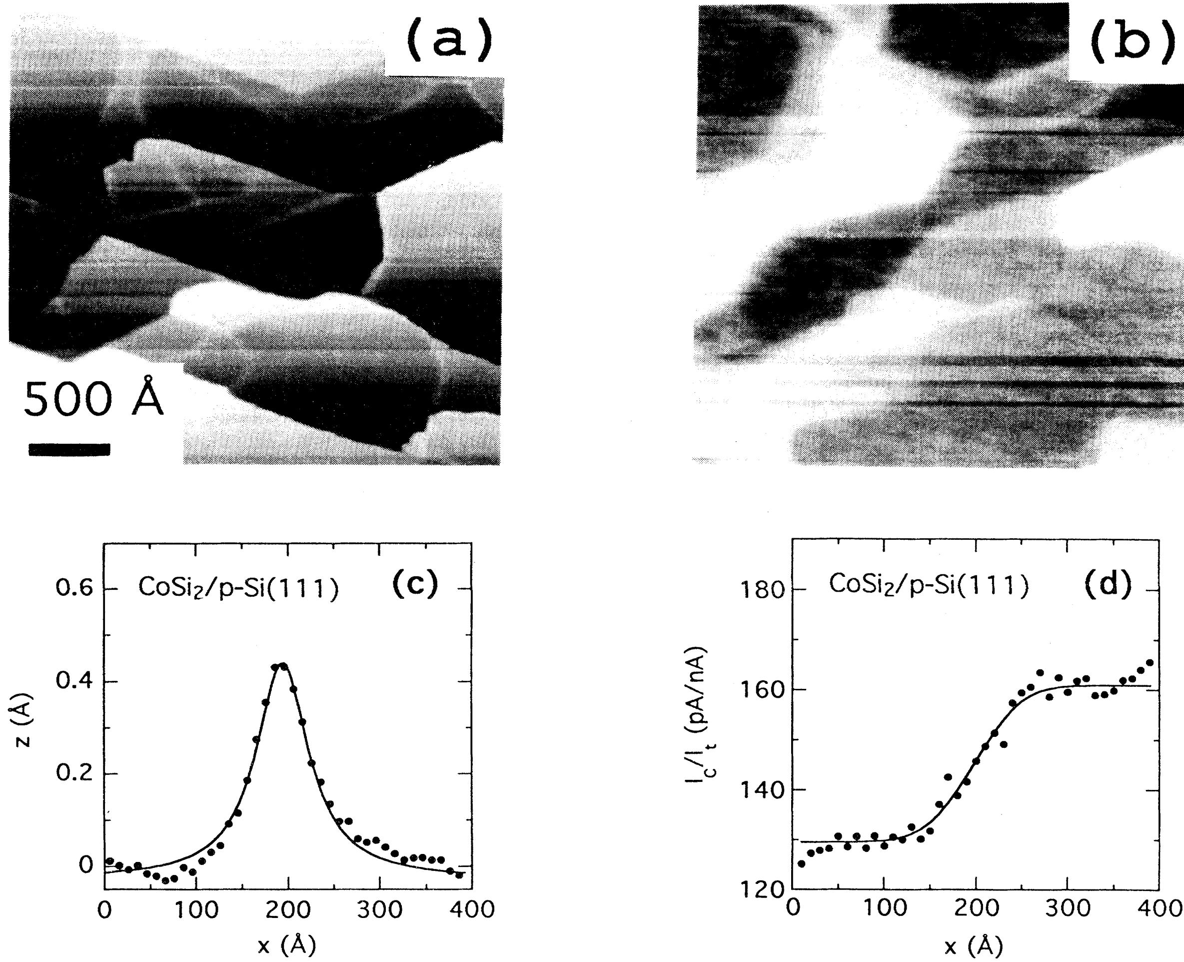

FIG. 11. (a) and (b) are a pair of simultaneously taken STM and reverse BEEM images of a 22-Å $CoSi_2$/*p*-type Si(111) over a 3000×3000-$Å^2$ area. Empty states were probed and $V=-6$ V and $I_t=6$ nA. Horizontal streaks in the images are due to instabilities of the STM tip. The STM gray scale ranges over 7.46 Å and the BEEM gray scale ranges from 572 (white) to 1480 pA (black). Note that the larger I_c appears darker here. Similar to forward BEEM (shown in Fig. 9), atomic thickness variations in the film give rise to the contrast in the BEEM image. (c) and (d) are an arbitrary pair of STM and BEEM line sections taken from the area shown in (a). The topography profile was fit to a Lorentzian, and the BEEM profile was fit to an erf function, as described in the text.

Extrapolating to zero thickness using the measured λ's, a factor of $\sim$4 difference in the TP's is predicted at zero thickness. However, the TP for $CoSi_2$/*p*-type Si(111) of same thickness was smaller, and this is attributed to an effect of the tunnel current distribution and a breakdown of the Stiles-Hamann theory for $V>0$. For $CoSi_2$/*n*-type Si(100), evidence of at least two different interfacial structures was found, consistent with an independent TEM investigation.

ACKNOWLEDGMENTS

Technical assistance from H.-J. Gübeli and C. Schwarz was invaluable during the earlier part of this work. One of us (E.Y.L) thanks M. D. Stiles for a useful explanation of his theory, and the Swiss National Science Foundation (NFP24) for financial support. Also, we acknowledge financial support from the Swiss Research Foundation for H.S., and from "Kommission zur Förderung der wissenschaftlichen Forschung" for U.K.

[1]W. J. Kaiser and L. D. Bell, Phys. Rev. Lett. **60**, 1406 (1988); L. D. Bell and W. J. Kaiser, *ibid.* **61**, 2368 (1988).
[2]L. D. Bell, W. J. Kaiser, M. H. Hecht, and L. C. Davis, in *Scanning Tunneling Microscopy,* edited by J. A. Stroscio and W. J. Kaiser (Academic, San Diego, 1993), pp. 307–348, and references therein.
[3]P. Niedermann, L. Quattropani, K. Solt, A. D. Kent, I. Maggio Aprile, and O. Fischer, Phys. Rev. B **48**, 8833 (1993).
[4]L. D. Bell, W. J. Kaiser, and M. H. Hecht (unpublished).
[5]R. Ludeke and A. Bauer, Phys. Rev. Lett. **71**, 1760 (1993).

[6]A. Bauer, M. T. Cuberes, M. Prietsch, and G. Kaindl, Phys. Rev. Lett. **71**, 149 (1993).
[7]L. J. Schowalter and E. Y. Lee, Phys. Rev. B **43**, 9308 (1991).
[8]J. J. Quinn, Phys. Rev. Lett. **126**, 1453 (1962).
[9]H. Sirringhaus, E. Y. Lee, and H. von Känel, Phys. Rev. Lett. **73**, 577 (1994).
[10]E. Y. Lee, H. Sirringhaus, and H. von Känel, Surf. Sci. Lett. **314**, L823 (1994).
[11]M. D. Stiles and D. R. Hamann, Phys. Rev. Lett. **66**, 3179 (1991).
[12]E. Y. Lee, H. Sirringhaus, and H. von Känel, Phys. Rev. B **50**, 14 714 (1994).
[13]L. D. Bell, *et al.*, Phys. Rev. Lett. **64**, 2679 (1990).
[14]M. Prietsch and R. Ludeke, Phys. Rev. Lett. **66**, 2511 (1991).
[15]R. Ludeke, Phys. Rev. Lett. **70**, 214 (1993).
[16]E. Y. Lee and L. J. Schowalter, Phys. Rev. B **45**, 6325 (1992).
[17]E. Y. Lee, H. Sirringhaus, and H. von Känel, Phys. Rev. B **50**, 5807 (1994).
[18]J. C. Inkson, J. Phys. C **4**, 591 (1971).
[19]C. J. Chen, J. Vac. Sci. Technol. A **6**, 319 (1988); J. A. Stroscio, R. M. Feenstra, and A. P. Fein, Phys. Rev. Lett. **57**, 2579 (1986).
[20]L. F. Mattheiss and D. R. Hamann, Phys. Rev. B **37**, 10 623 (1988).
[21]W. R. Lambrecht, N. E. Christensen, and P. Blöchl, Phys. Rev. B **36**, 2493 (1993).
[22]G. C. F. Newcombe and G. G. Lonzarich, Phys. Rev. B **37**, 10 619 (1988).
[23]J. C. Hensel, R. T. Tung, J. M. Poate, and F. C. Unterwald, Appl. Phys. Lett. **44**, 913 (1984); Phys. Rev. Lett. **54**, 1840 (1985).
[24]N. W. Aschcroft and N. D. Mermin, *Solid State Physics* (Saunders, Philadelphia, 1976), pp. 5 and 38ff.
[25]H. Sirringhaus, E. Y. Lee, and H. von Känel, J. Vac. Sci. Technol. B **12**, 2629 (1994).
[26]U. Kafader, H. Sirringhaus, and H. von Känel (unpublished); for a description of the technique, see J. Ramm, E. Beck, A. Züger, A. Dommann, and R. E. Pixley, Thin Solid Films **222**, 126 (1992).
[27]H. von Känel, Mater. Sci. Rep. **8**, 193 (1992), and references therein.
[28]C. W. T. Bulle-Lieuma, D. E. W. Vandenhoudt, J. Henz, N. Onda, and H. von Känel, J. Appl. Phys. **73**, 3220 (1993).
[29]R. Stalder, H. Sirringhaus, N. Onda, and H. von Känel, Appl. Phys. Lett. **59**, 1960 (1991).
[30]R. Stalder, H. Sirringhaus, N. Onda, and H. von Känel, Ultramicroscopy **42-44**, 781 (1992).
[31]F. R. N. Nabarro, *Theory of Crystal Dislocations* (Dover, New York, 1987), pp. 53ff.
[32]R. Stalder, C. Schwarz, H. Sirringhaus, and H. von Känel, Surf. Sci. **271**, 355 (1992).
[33]G. Simmons, J. Appl. Phys. **34**, 1793 (1963).
[34]N. D. Lang, A. Yacoby, and Y. Imry, Phys. Rev. Lett. **14**, 1499 (1989).
[35]A. M. Milliken, S. J. Manion, W. J. Kaiser, L. D. Bell, and M. H. Hecht, Phys. Rev. B **46**, 12 826 (1992).
[36]C. W. T. Bulle-Lieuwma, A. F. de Jong, and D. E. W. Vandenhoudt, Philos. Mag. A **64**, 255 (1991).
[37]M. H. Hecht, L. D. Bell, W. J. Kaiser, and L. C. Davis, Phys. Rev. B **42**, 7663 (1990).
[38]J. R. Jimenez, J.-C. Wu, L. J. Schowalter, B. D. Hunt, R. W. Fathauer, P. J. Grunthaner, and T. L. Lin, J. Appl. Phys. **66**, 2738 (1989).
[39]Note that the free-electron model B actually predicts a *smaller* λ than what is observed. Interband transitions would make the difference even larger.
[40]C. Chang, C. Hu, and R. W. Brodersen, J. Appl. Phys. **57**, 302 (1985); R. C. Alig, S. Bloom, and C. W. Struck, Phys. Rev. B **22**, 5565 (1980).

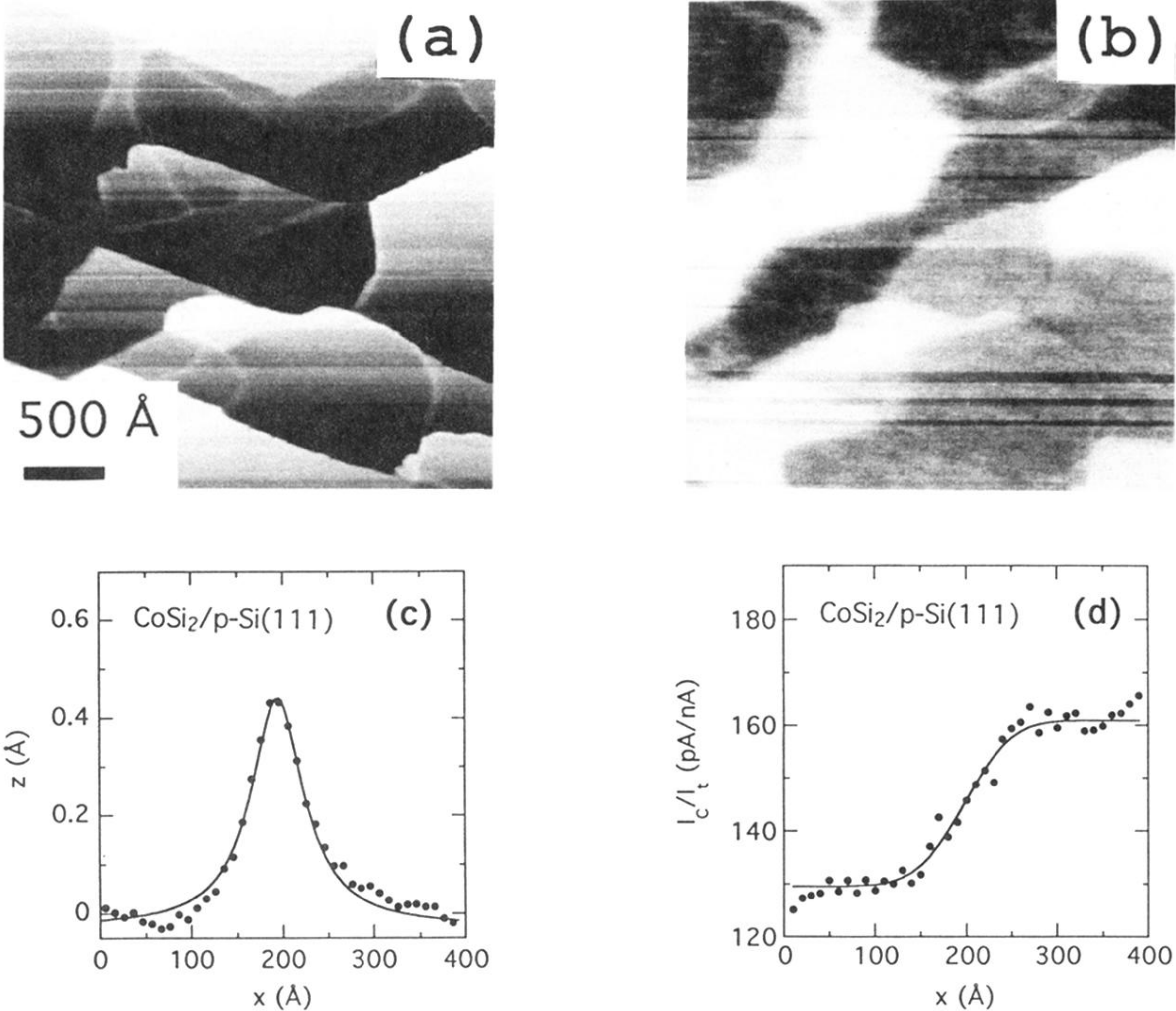

FIG. 11. (a) and (b) are a pair of simultaneously taken STM and reverse BEEM images of a 22-Å $CoSi_2$/*p*-type Si(111) over a 3000×3000-Å^2 area. Empty states were probed and $V=-6$ V and $I_t=6$ nA. Horizontal streaks in the images are due to instabilities of the STM tip. The STM gray scale ranges over 7.46 Å and the BEEM gray scale ranges from 572 (white) to 1480 pA (black). Note that the larger I_c appears darker here. Similar to forward BEEM (shown in Fig. 9), atomic thickness variations in the film give rise to the contrast in the BEEM image. (c) and (d) are an arbitrary pair of STM and BEEM line sections taken from the area shown in (a). The topography profile was fit to a Lorentzian, and the BEEM profile was fit to an erf function, as described in the text.

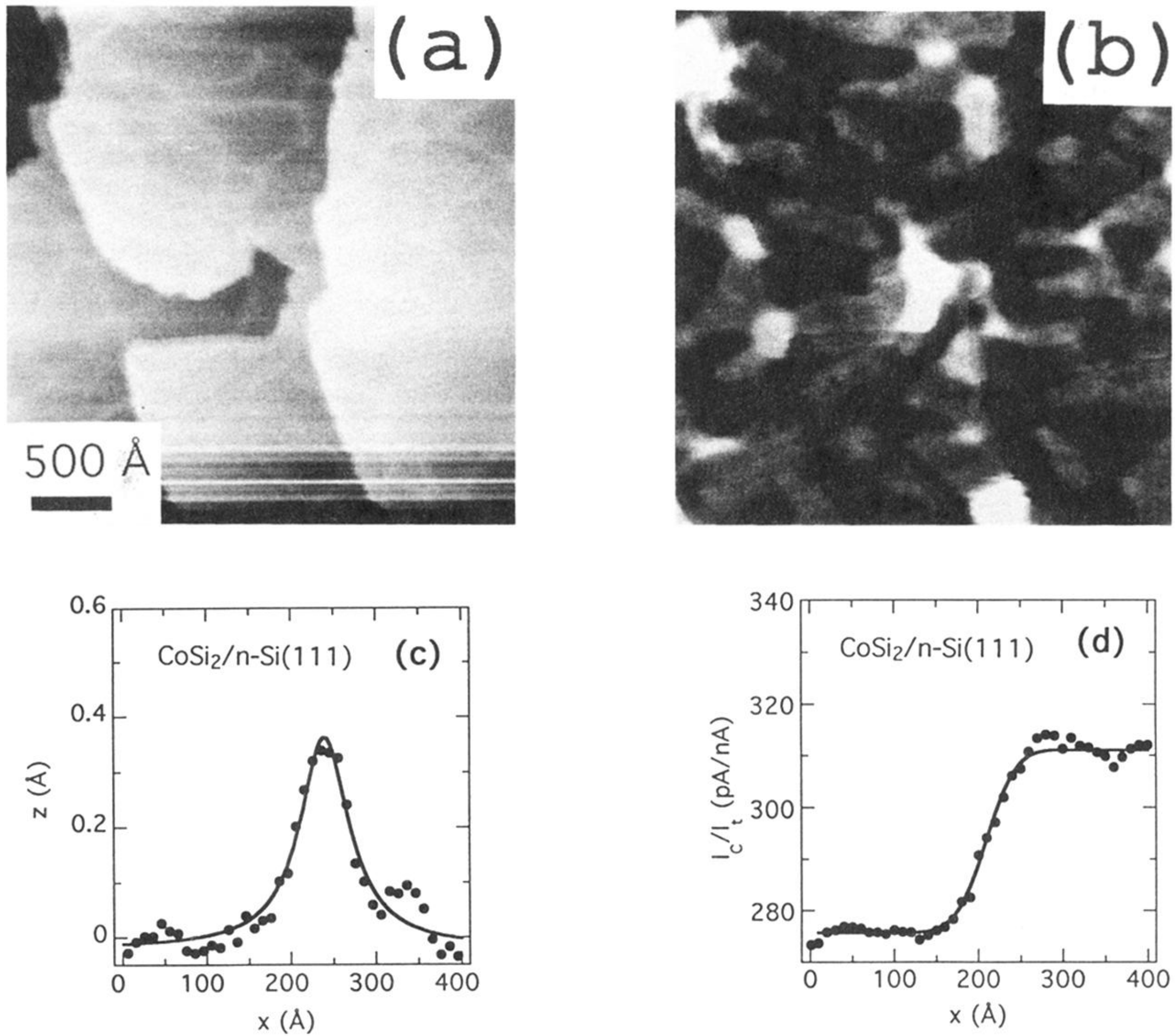

FIG. 9. (a) and (b) are a pair of simultaneously taken STM and forward BEEM images of a 22-Å $CoSi_2$/*n*-type Si(111) film over a 3000×3000-Å^2 area. Empty states were probed and $V=-6$ V and $I_t=2$ nA. The STM image shows three monolayer steps each 3.1 Å high, and a strain field due to dislocation appearing as a light network. The BEEM image shows atomic thickness variations of the film. The gray scale in the BEEM image is from 467 (black) to 736 pA (white). Areas appearing darker are thicker areas. (c) and (d) are an arbitrary pair of STM and BEEM line sections taken from the area shown in (a). The topography profile was fit to a Lorentzian, and the BEEM profile was fit to an erf function as described in the text.